Potential erosion capacity of gravity currents created by changing initial conditions

Zordan Jessica[1], Schleiss Anton J.[1], and Franca Mário J.[1,2]

[1]Laboratory of hydraulic constructions (LCH), School of Architecture, Civil and Environmental Engineering, École Polytechnique Fédérale de Lausanne (EPFL), 1015 Lausanne, Switzerland
[2]River Basin Development chair group, Water Science and Engineering department, IHE Delft Institute for Water Education, 2611 Delft, The Netherlands

Correspondence to: Zordan Jessica (jessica.zordan@epfl.ch)

Abstract. Gravity currents reproduced in laboratory by the lock-exchange technique are here tested for three initial densities and five lock-lengths, for horizontal and four inclinations of the lock. The main purpose is to quantify the effect of the introduction of an inclined channel reach just upstream from the lock gate, on the hydrodynamics of gravity currents and consequently on its transport capacity. The shape of the current is modified due to the enhanced entrainment of ambient water and the body is the region of the current where this most happens. A range of upstream slopes is tested, going from horizontal to a limit case in which two mechanisms compete, i.e. the current entrainment of water from the upper surface due to the increment of friction and the head feeding by a rear fed current. In particular, bed shear stress and the corresponding erosion potential are analysed. The implications of an inclined reach upstream of the lock gate on the potential entrainment capacity of the flow is here discussed.

1 Introduction

Spontaneous in nature or originated by human activities, many are the occurrences of gravity currents. These flows are created by differences in hydrostatic pressures at the surface of contact of two fluids with density differences. Temperature inhomogeneities cause the density gradient which is at the origin of katabatic winds, an example of the occurrence of gravity currents in the atmosphere. Avalanches of airborne snow, plumes of pyroclasts from volcanic eruptions and sand storms are atmospheric flows where suspended particles play a major role in producing the density gradient. If suspended sediment produces the extra density, gravity currents take the name of turbidity currents. Turbidity currents are of particular interest for reservoirs sedimentation, which have important economic costs due to the loss of volume for water storage (Palmieri et al. (2001), Schleiss et al. (2016)). Among gravity currents caused by human actions, the release of pollutants into rivers, oil spillage in the ocean and the desalination plants outflows are of primary importance due to their negative environmental impacts.

Gravity currents have been subjects of research over the last decades. Simpson (1997), Kneller and Buckee (2000), Huppert (2006) and Ungarish (2009) present a comprehensive review of the early work on natural and experimentally reproduced gravity currents. Recently Azpiroz-Zabala et al. (2017) provided a new model for the gravity current structure. They argued that real world turbidity currents in submarine canyons are characterized by a so-called "frontal-cell" which is highly erosive

and therefore able to self-sustaining itself and to outrun the slower moving body of the flow, creating a stretched current. Nevertheless, authors working on small scale experimentally reproduced gravity currents agree on describing the shape of the gravity current as composed by an arising highly turbulent front, called head, followed by, in some cases, a body and a tail. Particularly in the body, that can reach a quasi-steady state, a vertical structure can be distinguished. A gravity current presents two main interfaces where exchanges concur: at the bottom, generally a solid boundary, and at the top, at the interface with the ambient fluid. These are active boundaries where mass and momentum exchanges are promoted (Ancey, 2012). Ambient fluid is entrained due to shear and buoyancy instabilities at the upper interface (Cantero et al., 2008) resulting in the dilution of the underlying current and modification of the density profile which characterizes a gravity current under stable density stratification (Turner, 1973). If the gravity current travels above an erodible bed, entrainment of material from the bottom can take place, which is conveyed with the current and redeposited sometimes at large distances from their original position (Zordan et al., 2018a). High shear stress associated with intense ejection and burst events influence erosion and bed load transport (Niño and Garcia (1996), Cantero et al. (2008), Zordan et al. (2018a)). For example, in the shallow shelf region of the lake it is frequently observed that cold water, relatively denser than that in open waters, starts to descend down the slope as a cold gravity current (Fer et al., 2002). The plume is able to transport suspended sediment together with their dissolved components, oxygen, and pollutants into deeper water. A proper parametrization of both upper layer and bottom entrainment is still an open research field which needs to be addressed. Indeed, small variations in the entrainment parameters highly influence the flow dynamics (Traer et al., 2012).

Gravity currents can originate under different conditions: changes of initial volume of denser fluid and changes of the bottom inclination represent some of the various configurations that can be found in reality. To understand how lock-volume and lock-slope, which are initial trigger conditions of gravity currents, are linked with their transport capacity is thus of fundamental importance.

Gravity currents are here reproduced in laboratory by the lock-exchange technique. Three initial densities are tested in combination with five lock-lengths on horizontal bottom and with four inclinations of the upstream channel reach. The bottom of the channel was designed in order to have a variable slope angle of the lock and a following flat surface. The main purpose is to investigate how the increment of gravitational forces, due to the introduction of a slope in the lock, affect the hydrodynamic of gravity currents and consequently its transport capacity observed downstream in a flat reach.

Britter and Linden (1980) reproduced gravity currents down a slope with no breaks and he found a critical angle, which is typically less than a degree, over which buoyancy force is large enough to counter-act the bottom friction producing a steady flow. At larger slopes, two mechanisms affect the evolution of the current: the current entrains water from the upper surface due to the increment of friction and the head is fed by the rear steady current. Mulder and Alexander (2001) studied slope-break deposits created by turbidity currents. They said that the amount of mixing between flow and ambient fluid is influenced by slope changes which furthermore cause significant changes in turbidite thickness. In the present study the effect of a change in slope is analysed by testing a range of lock-slopes below 16% ($0° \leq \alpha < 9°$). It is expected that the two mechanisms mentioned by Britter and Linden (1980) take place in the lock for the depletion current here formed, due to the incremental gravitational

forces, so the transition from a friction governed flow to a flow in which gravitational forces become more and more important happens. The erosion potential of a gravity current formed under such varying initial conditions is then discussed.

The present paper is structured as such: first the experimental set-up and the process which allows for the noise reduction of the velocity measurements are described. Then, the results are presented: a method for the identification of the shape of the current is described and, by means of the mean streamwise velocity field, both bottom and interface shear stresses are computed. The variation on the shape caused by changing initial conditions (i.e. with different initial buoyancies, various lock-lengths and lock-bottom inclinations) are therefore discussed. The potential water entrainment and bottom erosion capacity are estimated on the base of the computed shear stresses evolutions. Finally, an overview of the main findings is presented in the conclusions.

2 Methodology

2.1 Experimental set-up

The tests are performed in a channel with a rectangular section, 7.5 m long and 0.275 m wide. The gravity currents are reproduced through the lock-exchange technique by sudden release of a gate which divides the flume in two parts where the fluids of different densities are at rest. Three buoyancy differences are tested in combination with five lock-slopes, ranging from $S = 0\%$ (horizontal bed) to $S = 16\%$ (tests S0 to S4). Figure 1 shows the configurations from horizontal bed (S0) to the steepest slope (S4). By introducing a slope on the channel lock reach, the volume of denser fluid is reduced. This lock contraction is also tested separately by performing reference tests with the combination of the three initial densities and the five lock-lengths which correspond to the very same volumes in the lock of the tests under inclined. The experimental parameters are reported in Table 1. $\mathrm{R}_i.\mathrm{S}_i$ refer to gravity currents reproduced by different initial density with the presence of a lock-slope while $\mathrm{R}_i.\mathrm{L}_i$ indicates the tests with varying initial density and lock-length.

The channel is filled with 0.2 m of ambient water in one side and of salty water, up to the same level, in the lock reach. Once the gate is removed, the saline current forms. At 2.5 m from the gate an Acoustic Doppler Velocity Profiler (ADVP) is placed to measure 3D instantaneous velocities along a vertical. The ADVP (Lemmin and Rolland (1997), Hurther and Lemmin (2001), Franca and Lemmin (2006)) is a non-intrusive sonar instrument that measures the instantaneous velocity profiles using the Doppler effect without the need of calibration and was used with an acquisition frequency of 31.25 Hz. The velocity profiles are collected in time along a fixed vertical. The flume is connected to a final big reservoir that allows the current dissipation and avoids its reflection upstream.

Normalization of the time is made using the scale $t^* = h_b/u_b$, where h_b is a vertical geometric scale, here considered as one third of the total height of the fluid in the experimental tank, h_0 ($h_b = h_0/3$ and $h_0 = 0.2$ m) and $u_b = \sqrt{g'h_b}$ is the buoyancy velocity.

S_i tests	ρ_0 $\left[\frac{kg}{m^3}\right]$	g'_0 $\left[\frac{m^2}{s}\right]$	u_0 $\left[\frac{m}{s}\right]$	Re_0 $[-]$	S [%]	α [°]	V_i/V_0
R1.S0	1028	0.29	0.24	48166	0	0.00	1.000
R1.S1	1028	0.29	0.24	48166	4	2.29	0.750
R1.S2	1028	0.29	0.24	48166	6	3.43	0.625
R1.S3	1028	0.29	0.24	48166	8	4.57	0.500
R1.S4	1028	0.29	0.24	48166	16	9.09	0.250
R2.S0	1038	0.39	0.28	55857	0	0.00	1.000
R2.S1	1038	0.39	0.28	55857	4	2.29	0.750
R2.S2	1038	0.39	0.28	55857	6	3.43	0.625
R2.S3	1038	0.39	0.28	55857	8	4.57	0.500
R2.S4	1038	0.39	0.28	55857	16	9.09	0.250
R3.S0	1048	0.49	0.31	62610	0	0.00	1.000
R3.S1	1048	0.49	0.31	62610	4	2.29	0.750
R3.S2	1048	0.49	0.31	62610	6	3.43	0.625
R3.S3	1048	0.49	0.31	62610	8	4.57	0.500
R3.S4	1048	0.49	0.31	62610	16	9.09	0.250

L_i tests	ρ_0 $\left[\frac{kg}{m^3}\right]$	g'_0 $\left[\frac{m^2}{s}\right]$	u_0 $\left[\frac{m}{s}\right]$	Re_0 $[-]$	L_i $[m]$	V_i/V_0 $[-]$
R1.L0	1028	0.29	0.24	48166	2.500	1.000
R1.L1	1028	0.29	0.24	48166	1.875	0.750
R1.L2	1028	0.29	0.24	48166	1.563	0.625
R1.L3	1028	0.29	0.24	48166	1.250	0.500
R1.L4	1028	0.29	0.24	48166	0.625	0.250
R2.L0	1038	0.39	0.28	55857	2.500	1.000
R2.L1	1038	0.39	0.28	55857	1.875	0.750
R2.L2	1038	0.39	0.28	55857	1.563	0.625
R2.L3	1038	0.39	0.28	55857	1.250	0.500
R2.L4	1038	0.39	0.28	55857	0.625	0.250
R3.L0	1048	0.49	0.31	62610	2.500	1.000
R3.L1	1048	0.49	0.31	62610	1.875	0.750
R3.L2	1048	0.49	0.31	62610	1.563	0.625
R3.L3	1048	0.49	0.31	62610	1.250	0.500
R3.L4	1048	0.49	0.31	62610	0.625	0.250

Table 1. Experimental parameters. ρ_0 is the initial density of the mixture in the upstream tank (measured with a densimeter), g' is the reduced gravity corresponding to ρ_0, $Re_0 = u_0 h_0/\nu_c$ is the Reynolds number based on initial quantities with $u_0 = \sqrt{g' h_0}$ the initial buoyancy velocity, $h_0 = 0.2$ m the total height of the water column and ν_c the kinematic viscosity of the denser fluid, α is the angle of inclination of the bottom in the lock, S is the lock-slope expressed in percentage (h_{S_i}/L_0, with h_{S_i} the height as in Figure 1), L_i is the length of the upstream lock-reach, V_i/V_0 the percentage of volume of the upstream lock-reach with respect to the configuration L_0.

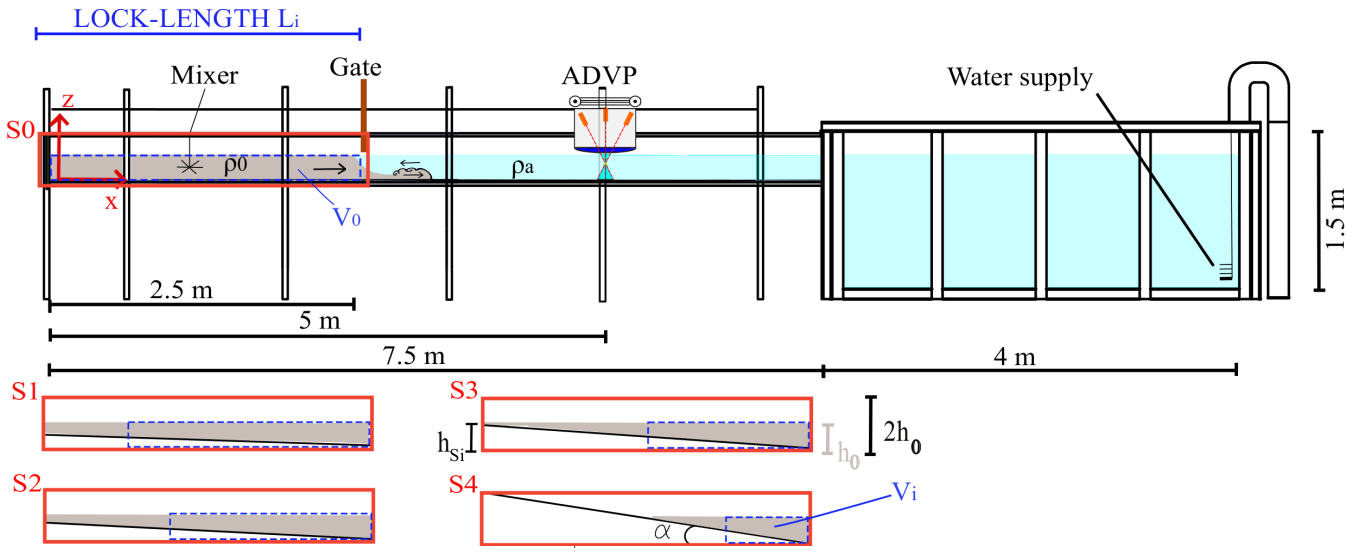

Figure 1. Longitudinal view and cross-section of the experimental set-up showing tested slope configurations S0 to S4 of lock volumes V_i.

2.2 Data filtering

By means of the analysis of the power spectra of the raw data collected with the ADVP, noisy frequencies were mainly detected below 8 Hz. The instantaneous measurements were thus low-pass filtered with 8 Hz as cut-off frequency (Zordan et al., 2018a). The 8 Hz cut-off has been chosen because the signal, for frequencies higher than 8 Hz, showed white noise. The time-series of the mean streamwise and vertical velocities ($\overline{u}$ and $\overline{w}$) for the unsteady gravity current, were derived after a filtering procedure that consisted in the application of a moving average over a time-window which is chosen by the analysis of the power spectra distribution as in Baas et al. (2005). This analysis showed that for a time window of 0.32 s, the harmonics of all the meaningful frequencies were still recognisable while, increasing the time window, the harmonics of progressively smaller frequency gradually lose power and they become impossible to distinguish (Baas et al., 2005). Thus, this window length was chosen for the moving average defining $\overline{u}$ and $\overline{w}$. The turbulent fluctuation time series (u' and w') is then calculated using the Reynolds decomposition:

$$u = \overline{u} + u' \tag{1}$$

where u is the instantaneous velocity. The cleaning procedure with the velocity signals and corresponding spectra is shown in Figure 2.

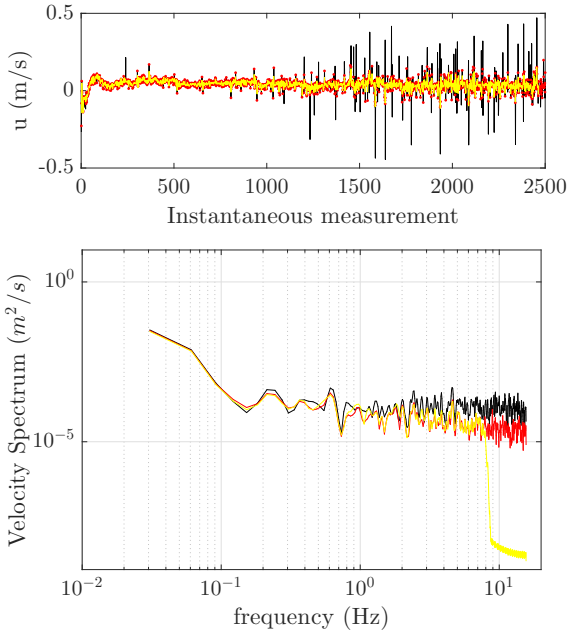

Figure 2. Raw velocity data (black) and despiked data (red) obtained with the procedure proposed by Goring and Nikora (2002). Then, through the analysis of the velocity spectra (figure at the bottom), the cut-off frequency of 8 Hz has been identified in order to low pass filter the noisy frequencies (yellow line).

3 Results

3.1 The shape of the current

A definition that allow to distinguish the head and the body regions of the current is considered. Once those regions are univocally identified, the estimation of the influence of the slope on the variation of the shape and extension of head and body regions will therefore be possible. In particular, a criterion is here established to identify the two main regions of a gravity current: the head and the body. The head and the body can be distinguished by different velocity fields and shape These distinctive features (a characteristic velocity and the contour of the current) have therefore been considered to identify the regions of the currents. A kinematic function (H) is defined and computed as the product between the instantaneous depth averaged streamwise velocity, $u_d(t)$:

$$u_d(t) = \frac{1}{h}\int_0^h u(z,t)dz \tag{2}$$

and the current height, $h(t)$, that is here identified by the position where the streamwise velocity is equal to zero, as in Zordan et al. (2018a). H is thus defined as:

$$H(t) = u_d(t)h(t) \tag{3}$$

By dimensional analysis, the function H corresponds to a flow rate per unit width. The head of the gravity current is characterized by a high specific flow rate which decreases at the rear of the head, a region where fluid is recirculated through vortical movements.

Nogueira et al. (2014) adopted a similar procedure to identify the head region by considering the product of the depth averaged streamwise velocity with the depth averaged density of the current. Therefore, the downstream limit of the head (L_h) is identified by the first meaningful local minimum of the function H, starting from the front.

Here L_h identifies the temporal extension of the head. The conversion from time to length scale may be done by using Taylor frozen hypothesis and considering a reference velocity of the current velocity as advection velocity. This method is coherent for all the experiments performed and the value of the H function is shown in Figure 3.

The body length is instead analysed by using the cumulative sum of the function H. This is a region where a quasi-steady regime is established for a certain time length. This implies that $\sum H$ shows a linear increment in time. The limit of the body is therefore defined by analysing the linear evolution that is fitted by a linear regression with least squares method for progressively longer portion of the accumulated summed data. The analysis of the development of R^2 value, the coefficient of determination, allows to find the extension of the linear portion which corresponds to the temporal extent of the body region (L_b). R^2 is defined as the square of the correlation between the response values and the predicted response values. It is computed as the ratio of the sum of squares of the regression (SSR) and the total sum of squares (SST) as:

$$R^2 = \frac{SSR}{SST} = \frac{\sum_{i=1}^{n}(y_i - \hat{y}_i)^2}{\sum_{i=1}^{n}(y_i - \bar{y}_i)^2} \tag{4}$$

where $\bar{y}$ is the average of the response y, $\hat{y}$ is the regression line an n the number of observations i. In Figure 3 the development of the function H is shown for the tests with the lock-slope. The same procedure is adopted for tests R_i.L_i and the results can be find in Zordan et al. (2018b).

The form of the currents was identified by the zero streamwise velocity contour. In Figure 4 the contours of each test with the lock-slope are compared with the correspondent reference test with lock-length variation. The results are grouped by the initial density on the lock (columns in the figure), and by pairs of tests with the same volume of the lock but for different slopes. The extension of head and body as identified by the previous methods are also reported with the vertical lines. Dashed lines refers to tests S_i while continuous lines correspond to L_i tests.

In Figure 4 we can see that the head of the currents does not show any relevant change. Instead the extension of the body is affected: it reduces with increasing inclination of the upstream channel reach and the same goes for tests produced by reduced

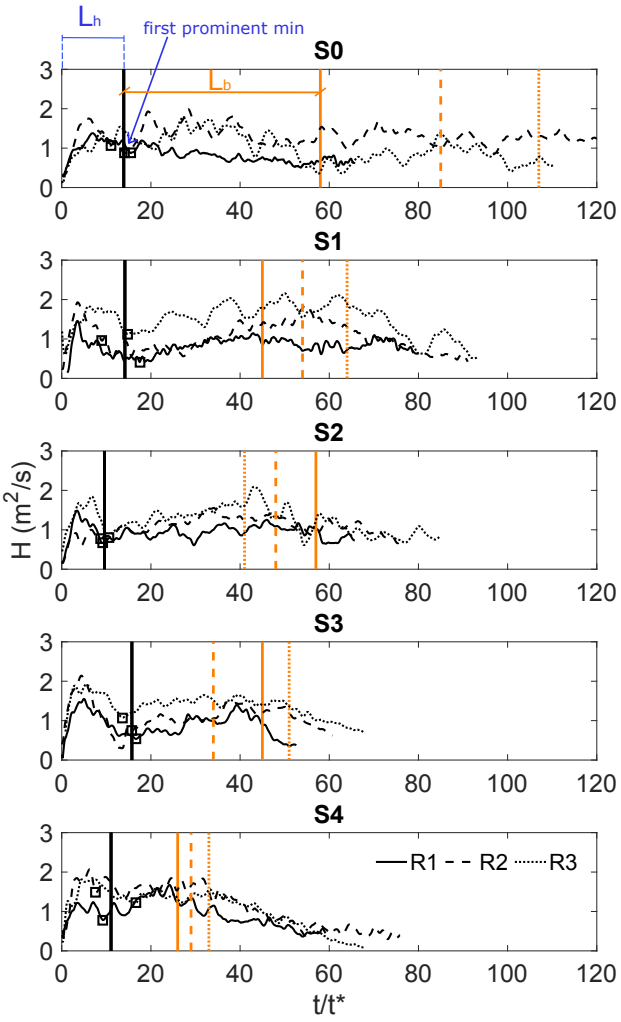

Figure 3. Determination of the gravity current head extension from the first prominent minimum of the function H (L_h). The extension of the body (L_b), as identified by the cumulative sum of the depth-averaged streamwise velocity, is also traced with the red vertical lines.

lock volume. A dependency on the initial density is noticed and in three out of the total five slopes bring to the formation of longer body with greater initial buoyancy. This can be verified in Figure 3 where extensions of the bodies are plotted with the vertical orange lines. R1, R2 and R3 produces progressively longer bodies for tests S0, S1 and S4.

The largest deviation between the two contours of corresponding tests L_i - S_i is noticed for the last configuration, with the R_i.L4 tests showing a shorter body and a more defined tail while for the correspondent tests with the inclined lock the body is more extended.

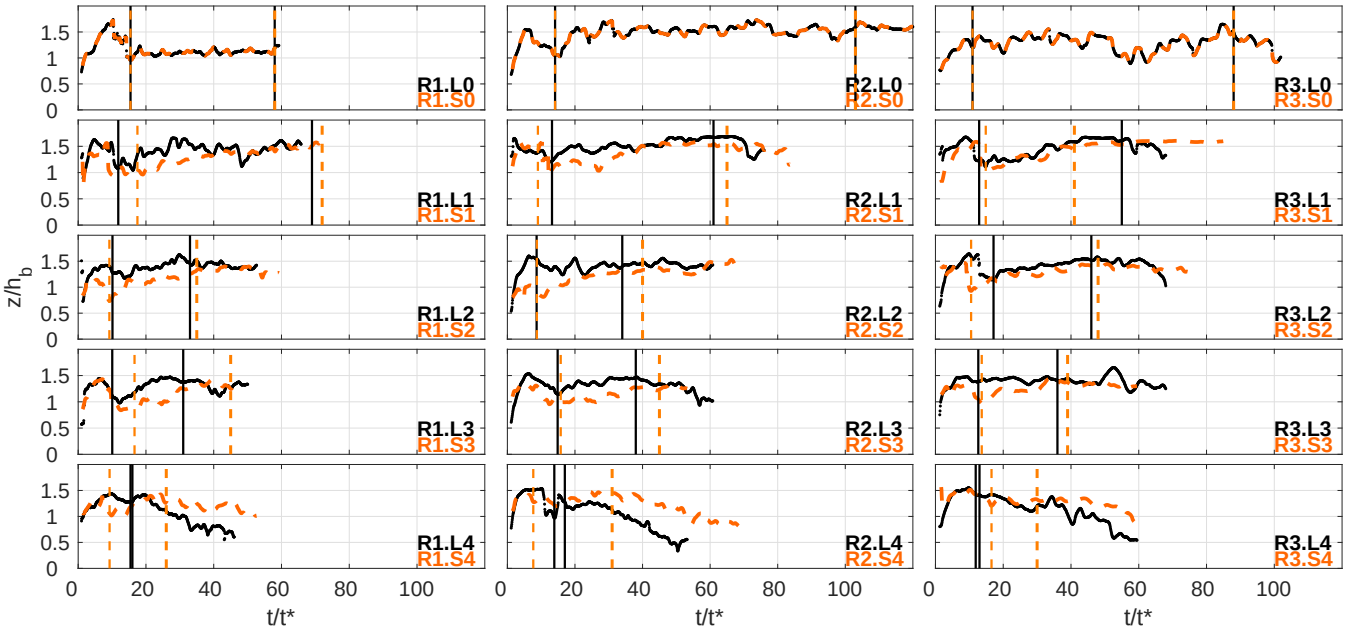

Figure 4. Gravity currents contours, as identified by the zero streamwise velocity contour, for tests with the lock-slope and correspondent tests with lock-length variation.

3.2 Mean velocity field

In Figure 5 the mean streamwise velocity field on the background and velocity vectors of the components ($\overline{u}$, $\overline{w}$) are shown for all the tests performed. The heads of the currents are indicated by the vertical dashed lines and the zero streamwise velocity contours are marked by the black lines. We can notice that the structures of the currents are quite similar in all configurations. An arising head is followed by a zone of high mixing, characterized by the presence of billows (due to Kelvin-Helmholtz type of instabilities (Simpson, 1972)) that are due to shear at the rear part of the elevated head. Body and tail are not always well defined regions, mainly for the class of tests down an inclined, and therefore the contour is not drawn. Moreover, tests S_i show lower streamwise velocities within head and body with respect to correspondent L_i tests.

By comparing tests S_i with the correspondent L_i tests, which have the same lock-volume but are performed without upstream slope, it is noticed that mean streamwise velocity is slightly higher for tests on horizontal bed. This can appear to some extent contradictory but that behaviour has already been mentioned in literature, in the study of Beghin et al. (1981), who was one of the first to investigate the role of the slope on the physics of a gravity current. He showed that tests which flows on small slopes, for tests where the entire channel was inclined, (typically less than 5°) experience a first acceleration phase followed by a deceleration phase. This is because of the fact that, although the gravitational force increases as the lock-slope becomes more inclined, there is also increased entrainment, both into the head itself and into the flow behind. This produces an extra dilution of the current with a decrease in buoyancy.

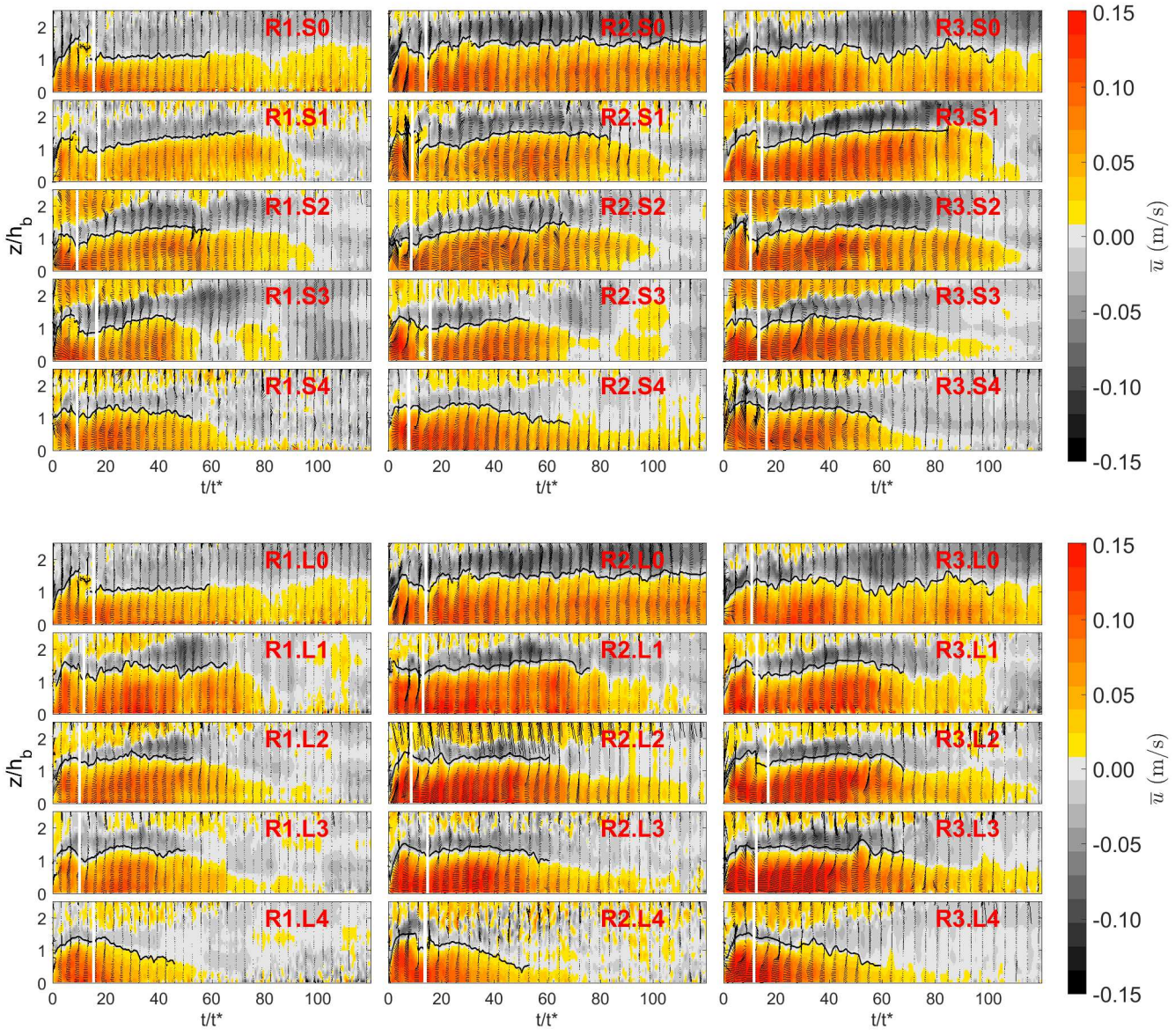

Figure 5. Streamwise velocity field on the background and velocity vectors of the components (u,w). The head of the current is delimited by the vertical white line. The contour of the current is indicated in black.

3.3 Bottom and upper shear stress

The sedimentological impact of a gravity current is the result of the complex hydrodynamic of this flow. Sediment entrainment is a complex mechanism mainly due to the difficulty in defining the fluctuating nature of turbulent flow (Salim et al., 2017). In

Zordan et al. (2018a) the transport of sediment within a gravity current is linked to the bed shear stress, that is here considered a "surrogate" measure of it. The form that bed shear stress is affected by the changing initial conditions of the current explains thus how the entrainment capacity of a current is altered. Bed shear stress temporal evolution is calculated by following the procedure in Zordan et al. (2018a) where it was assumed that the mean flow met the conditions necessary for the fitting of the overlapping layer by the logarithmic law of the wall as (Ferreira et al., 2012):

$$\frac{\overline{u}(z)}{u_*} = \frac{1}{k}\ln\frac{z}{z_0} \tag{5}$$

where $\overline{u}(z)$ is the mean velocity, u_* is the friction velocity, which is the velocity scale corresponding to the bed shear stress (Chassaing, 2010), k is the von Kármán constant, z is the vertical coordinate and z_0 is the zero-velocity level.

The equation of the logarithmic law of the wall can be rewritten as:

$$u = Aln(z) - B \tag{6}$$

where

$$A = \frac{u_*}{k},\ \ B = \frac{u_*}{k}ln(z_0) \tag{7}$$

Then, by determining the coefficients A and B through a fitting procedure, one obtains an estimation of u_* which is the velocity scale corresponding to the bed shear stress.

Bed shear stress is afterwards computed by considering a constant initial density that is here equal to the initial density in the lock (ρ_c):

$$\tau_b = \rho_c u_*^2 \tag{8}$$

The fitting procedure of the bottom logarithmic layer was determined stepwise, extending a linear least square fitting range (in a semi-logarithmic scale) from the lowest measured point until the maximum velocity vertical position. Then, within this region, the sublayer which provided the best regression coefficient was chosen and considered for the estimation of u_*, corresponding to the extent of the logarithmic layer as it was shown in Zordan et al. (2016).

The flow boundary is assumed to be smooth, as verified by a shear Reynolds number (or skin roughness, k_s, normalized by the viscous layer) is lesser than 5 (Nezu et al., 1994):

$$\frac{k_s u_*}{\nu} \leq 5 \tag{9}$$

The classic value of the von Kármán constant of $k = 0.405$ is adopted. Discussion on the estimation of k can be found in Ferreira (2015).

The bed shear stress time-evolution of gravity currents with lock-slope ($\tau_{b,S}$) are compared to the analogous results for tests with decreasing lock ($\tau_{b,L}$). Therefore the time-averaged bed shear stress has been computed and the ratio $\overline{\tau_{b,L}}/\overline{\tau_{b,S}}$ is shown in Figure 6. Tests performed with a lock-slope show in average lower values of bed shear stress ($\overline{\tau_{b,L}}/\overline{\tau_{b,S}} \geq 1$). By increasing the lock-slope this tendency is less evident and the mean bed shear stress compares for both conditions with varying

lock-slope and with different lock-lengths. Moreover, tests performed with the highest density difference seem less affected by changing configuration (S_iL_i with $i = 1, 2, 3, 4$). The detailed time series for this condition are presented in Figure 8, where we can see that from normalized time $t/t^* \simeq 20$, i.e. in the body region, bed shear stress is slightly higher for tests S_i than in the correspondent L_i tests.

At the upper boundary of the gravity currents, i.e. the interface with the ambient water, studies on turbulent flow near a density interface confirmed that under certain conditions, the turbulent boundary layer theory can be applied as well (Lofquist (1960), Csanady (1978)) and that the "law of the wall" can be applied to estimate the shear stress here. By hypothesizing a constant mean value of water viscosity and hydraulically smooth conditions, the estimation of an interface shear stress (τ_m) is made; qualitatively the estimation that will result is enough for the purpose of the present study. The time evolution of interface shear stress is therefore computed following the same procedure as for the bottom shear stress. In this case the fitting procedure of the logarithmic layer is determined by considering the mixing layer as defined in (Zordan et al., 2018b). This layer is delimited at the top by the zero streamwise velocity contour and at the bottom by the height of the current as defined by the Turner's integral scales (Ellison and Turner, 1959). Within this layer the at-least-three consecutive measurement points along the velocity profile which were giving the highest R^2 were considered for fitting. The time-average of the interface shear stress are compared by means of the ratio $\overline{\tau_{m,L}}/\overline{\tau_{m,S}}$ (Figure 7) showing that in general tests performed with varying lock-lengths present higher values with respect to correspondent tests with lock-slope variation i.e. $\overline{\tau_{m,L}}/\overline{\tau_{m,S}} \geq 1$.

Again the main differences between tests with reduced lock and respective tests with lock-slope are for the fourth configuration which detailed time-series are shown in Figure 9. The steepest slopes present higher values of interface shear stress in the body region with respect to the correspondent tests with the same initial volume of release but flowing on a horizontal bed.

4 Discussion

4.1 Shape variation of gravity current with the lock-slope

The extensions of the body of correspondent tests performed with the lock-slope or with horizontal bed, and with varying lock-lengths are compared in Figure 10. For lower lock-slopes the body extension is similar to the currents produced with the same lock-volume but with horizontal bottom. However, for lock-slopes at 16%, the body region for tests S_i are longer than correspondent tests L_i. At this point two mechanisms affect the evolution of the current: the current entrains water from the upper surface due to the increment of friction between the denser flow and the counter current progressively advancing upwards the lock, and the head is fed by the rear current. The flow of tests S4 show that the characteristics of the upstream flow in the lock are influencing the flow even when the current reaches the measuring point: (i) an extended body is the result of water entrainment at the upper surface of the current that creates dilution and expansion of the fluid in the current; (ii) the fluid in the body become faster as a result of the gravitational forces as in Britter and Linden (1980) (Figure 5). Britter and Linden (1980) showed that for currents flowing along a horizontal boundary, the head is the controlling feature. However down a slope, the body becomes more determinant in the gravity current evolution since it is up to 30-40$\%$ faster than the head velocity, depending on the slope, being able therefore to move faster fluid into the head. In our study, the lock-slopes 16%

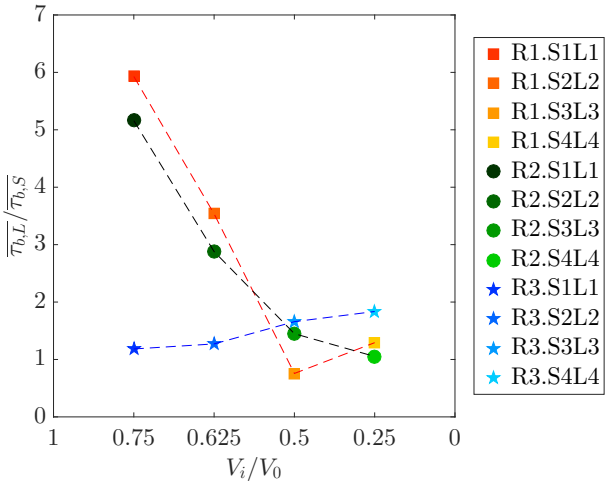

Figure 6. Ratio between time-averaged bed shear stress of respectively tests with varying lock-lengths ($\overline{\tau_{b,L}}$) and test with varying lock-slopes ($\overline{\tau_{b,S}}$). Dashed lines link tests performed with the same initial excess density while on the x-axis are the different configurations characterized by the percentage of volume of the upstream lock-reach V_i/V_0.

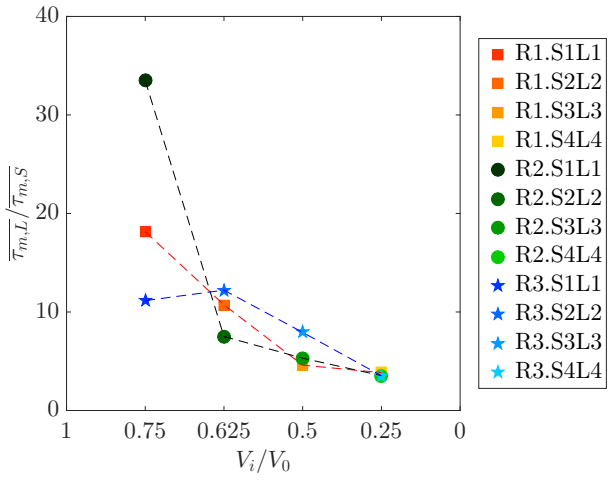

Figure 7. Ratio between time-averaged interface shear stress of respectively tests with varying lock-lengths ($\overline{\tau_{m,L}}$) and test with varying lock-slopes ($\overline{\tau_{,,S}}$). Dashed lines link tests performed with the same initial excess density while on the x-axis are the different configurations characterized by the percentage of volume of the upstream lock-reach V_i/V_0.

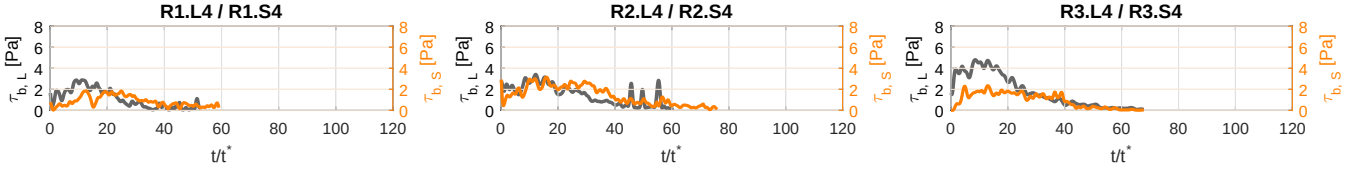

Figure 8. Temporal evolution of bed shear stresses calculated by log law fitting for tests with progressively reduced lock-length ($\tau_{b,L}$) and with the lock-slope ($\tau_{b,S}$).

show those features and the effect is not only occurring within the inclined lock but is also observed in the downstream flat part of the channel.

4.2 Ambient fluid entrainment

Kelvin-Helmholtz instabilities have a major role in provoking water entrainment. They take the form of vortical movements generated due to velocity shear at the interface between the two fluids. Since shear stress is determinant in the process of water entrainment, a new quantity to account for the potential entrainment capacity of the gravity current is here defined on the base of the computed time evolution of the interfacial shear stress (τ_m). It is computed as the non-dimensional time integral of the shear stress which represents, after dimensional analysis, the work done over a determined duration, per unit surface for a given

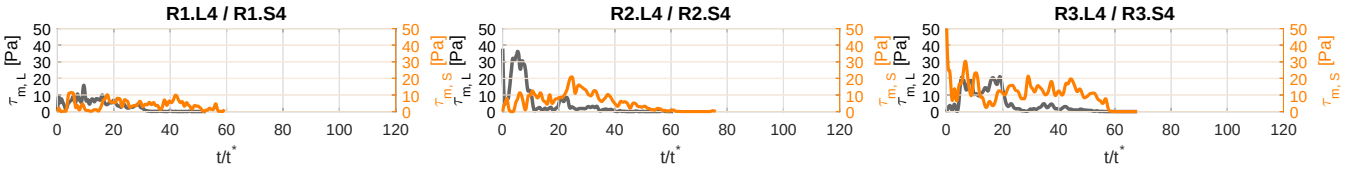

Figure 9. Temporal evolution of interfacial shear stresses calculated by log law fitting for tests with progressively reduced lock-length ($\tau_{m,L}$) and with the lock-slope ($\tau_{m,S}$).

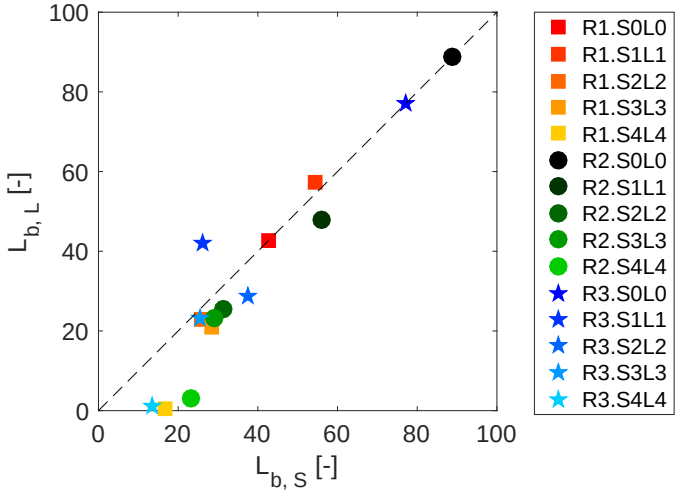

Figure 10. Comparison of the length of the body (L_b) between tests with progressively reduced lock-length and with lock-slope. The dashed line is the identity line.

advection velocity, which can be approximated as the initial buoyancy velocity, u_0. This quantity Φ_m is calculated as:

$$\Phi_m = \int_{T_1}^{T_2} \tau_m(t) dt / t^* \tag{10}$$

where the limits of integration are $T_1 = L_h$ and $T_2 = L_b$, in order to focus on the body, the region that has been found mostly affected by the variation of the initial conditions. The validity of the use of Φ_m as an indicator of the entrainment capacity is supported by the analysis of its relation with the Richardson number Ri (Zordan et al., 2018b). The relation between water entrainment and bulk Richardson number is well known in literature and numerous empirical fits to the experimental data have been proposed since the early work of Parker et al. (1987) and supported by more recent contributions (Stagnaro and Pittaluga, 2014). Therefore, it is here proposed to use this quantity as a surrogate for water entrainment capacity since it benefits from the instantaneous measurements of shear stress and therefore account for the unsteady behaviour of the gravity currents. In Figure 11, the potential water entrainments for gravity currents performed on an inclined and correspondent tests with reduced initial

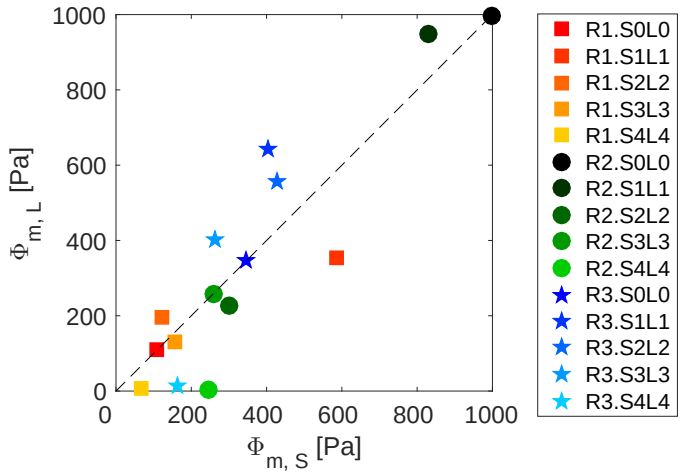

Figure 11. Comparison of Φ_m, a surrogate for the entrainment capacity of the mixing region, between tests with lock-slope (S_i) and correspondent tests on horizontal bottom (L_i). The dashed line is the identity line.

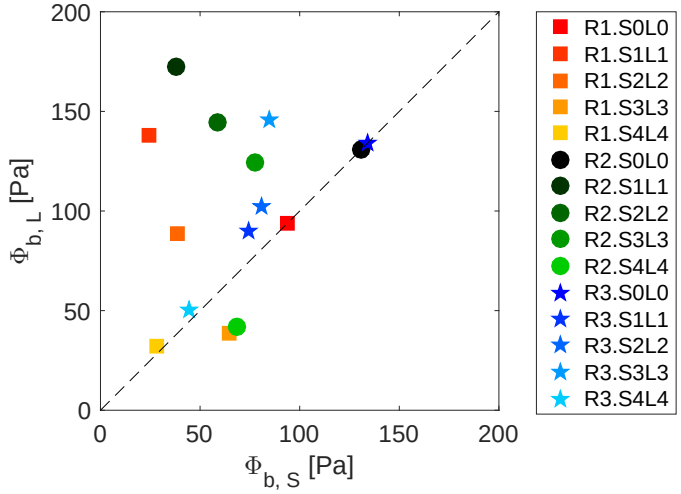

Figure 12. Comparison of the bottom erosion capacity Φ_b between tests with lock-slope (S_i) and correspondent tests on horizontal bottom (L_i). The dashed line is the identity line.

volume of release are compared. The tests S4L4 detach from the identity line, thus a greater water entrainment is expected for the case with the inclined bed with respect to the horizontal bottom.

4.3 Bottom erosion capacity

The magnitude of the shear stress at the lower boundary layer determines the sediment transport capacity of saline currents and whether erosion or deposition processes dominate the regime at the bottom boundary (Cossu and Wells, 2012). Therefore,

similarly to the interfacial water entrainment capacity, the bottom entrainment capacity, that can also be called the erosion capacity, is here computed on the base of the computed bed shear stress.

This new quantity is defined as:

$$\Phi_b = \int_{T_1}^{T_2} \tau_b(t) dt / t^* \tag{11}$$

where the limit T_i are $T_1 = 0$, $T_2 = L_b$.

In Zordan et al. (2018a) this quantity has been estimated for gravity currents simulated in presence of an erodible bed. A relationship between the eroded volume of sediments provoked by the passage of the gravity current and Φ_b has been found, therefore confirming that Φ_b is a good estimator of the entrainment capacity of these flows.

The bottom erosion capacity is compared for gravity currents performed with the lock-slope and correspondent tests on a horizontal bottom. Generally, L_i tests show a higher erosion capacity with respect to their analogous S_i. The points in Figure 12 are in fact concentrated above the bisect of the first and third quadrants. The effect of an extra gravitational force occurring in the flow upstream the lock, as described above, is proved not to play a role in enhancing the capacity of the current to perform bottom erosion, in the downstream flat reach of the channel, which is instead reduced. This is probably a consequence of the decrease in streamwise velocity which results from the dilution of the gravity current occurring already in the lock. On the other hand, ambient water entrainment causes the expansion of the body region. Longer bodies keep eroding material longer and the erosion potential attributed to this part is therefore increasing. The potential bottom erosion, i.e. the quantity Φ_b in Figure 13, shows a tendency to decrease with increasing lock-slope. This is mainly the result of the released volume reduction caused by the presence of the lock-slope, therefore originating shorter current bodies. The role of the body in the total erosion capacity is computed as the ratio Φ_{b-body}/Φ_b (Figure 13) whose limits of integration of Φ_{b-body} are $T_1 = L_h$ and $T_2 = L_b$. The contribution that is ascribed to the body has a similar development as the total erosion capacity. This enforce the hypothesis that the body is determinant in the entrainment capacity of a gravity current. Figure 13 highlights that the importance of the body in the total erosion capacity becomes proportionally higher for tests S4 (the trend lines in Figure 13 deviates more in this configuration). Higher water entrainment was proved in Section 4.2 for this latter case, which was therefore subjected to an expansion of the body region. An influence of the upper surface on the dynamics of the lower bottom boundary is therefore hypothesized. The interaction between the upper layer and the bottom was already pointed out by the numerical investigation of Cantero et al. (2008) and experimental evidences were reported in Zordan et al. (2018b). In this latter the vorticity was analysed showing that residual negative vorticity expands from the upper layer through the bottom with progressively lower intensity.

5 Conclusion

In most practical situations gravity currents are flowing on different topographies and most of the time travels along inclined but discontinuous slopes (slope breaks). Moreover they are generally originated by the release of a certain amount of a fluid

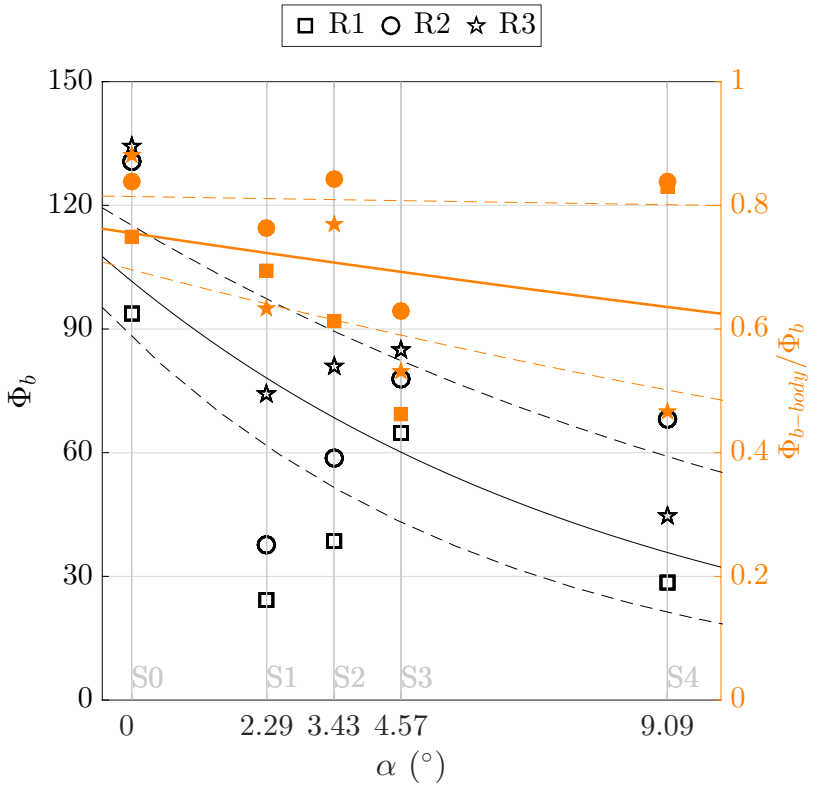

Figure 13. Potential erosion capacity for gravity currents (left axis) developed with different lock-inclinations and rate of potential bottom erosion due to the body of the gravity current on the total bottom erosion capacity, $\Phi_{b-body}/\Phi b$, (right axis). The exponential fitting lines are reported in order to give evidence of the general trend, together with the 85% confidence intervals (dashed lines).

of various densities. The present study analyses all the previously mentioned changing initial conditions which trigger gravity currents that are commonly observed in nature.

In this paper the effect on a downstream flat propagating reach, of incremental gravitational forces induced in the current which is formed still upstream in the lock is tested by reproducing experimentally gravity currents of different initial densities with the presence of an inclined lock. Corresponding tests with a horizontal lock are performed as well in order to have the reference cases with reduced volume. The range of lock-slopes tested varies from horizontal bed to $S = 16\%$ (which correspond to an inclination of the lock $\alpha \approx 9°$). The gravitational force is the main driving force which directly depends on slope (Khavasi et al., 2012). Therefore, at the upstream inclined reach which constitutes the lock, there is the action of gravitational forces which compete with the entrainment that takes place due to higher shear stress at the upper interface and tend to dilute the current. Thus, if on one hand gravitational acceleration drives for a faster gravity current, on the other hand water entrainment at the upper interface dilute the fluid of the current which is consequently slowed down and it expands due to the incorporation of the ambient fluid. The configurations S4-L4, corresponding to the steepest lock-slope and the shortest lock-length, respectively, exhibit the highest deviations in terms of shape and ambient water entrainment between tests with

lock-slopes with respect to correspondent tests on the horizontal bed. S4 tests showed a longer body, owing to entrainment of the ambient fluid. Bottom erosion capacity at the downstream flat reach is reduced by the presence of the extra gravitational forces, most probably due to lower streamwise velocities which are consequence of gravity currents dilution occurring on the way of the gravity current along the channel. The limit case of tests S4, with a lock-slope of $S = 16\%$, is the transient condition as described by previous literature for a continuously sloped channel (Britter and Linden (1980), Beghin et al. (1981), Parker et al. (1987), Maxworthy and Nokes (2007), Maxworthy (2010)), where buoyancy force is large enough to counter-act bottom and upper layer frictions. The limit given by the experimental set up did not allow to go for steeper lock-slopes, cases for which therefore further investigation should be undertaken.

Competing interests. The authors have no conflict of interest to declare.

Acknowledgements. This research was funded by the European project SEDITRANS funded by Marie Curie Actions, FP7-PEOPLE-2013-ITN-607394 (Multi partner - Initial Training Networks).

References

Ancey, C.: Gravity flow on steep slope, vol. Buoyancy Driven Flows, Cambridge University Press New York, 2012.

Azpiroz-Zabala, M., Cartigny, M. J., Talling, P. J., Parsons, D. R., Sumner, E. J., Clare, M. A., Simmons, S. M., Cooper, C., and Pope, E. L.: Newly recognized turbidity current structure can explain prolonged flushing of submarine canyons, Science Advances, 3, e1700 200, 2017.

Baas, J. H., McCaffrey, W. D., Haughton, P. D., and Choux, C.: Coupling between suspended sediment distribution and turbulence structure in a laboratory turbidity current, Journal of Geophysical Research: Oceans, 110, 2005.

Beghin, P., Hopfinger, E., and Britter, R.: Gravitational convection from instantaneous sources on inclined boundaries, Journal of Fluid Mechanics, 107, 407–422, 1981.

Britter, R. and Linden, P.: The motion of the front of a gravity current travelling down an incline, Journal of Fluid Mechanics, 99, 531–543, 1980.

Cantero, M. I., Balachandar, S., García, M. H., and Bock, D.: Turbulent structures in planar gravity currents and their influence on the flow dynamics, Journal of Geophysical Research: Oceans, 113, 2008.

Chassaing, P.: Mécanique des fluides, Cepadues éditions, 2010.

Cossu, R. and Wells, M. G.: A comparison of the shear stress distribution in the bottom boundary layer of experimental density and turbidity currents, European Journal of Mechanics, B/Fluids, 32, 70–79, https://doi.org/10.1016/j.euromechflu.2011.09.006, http://dx.doi.org/10.1016/j.euromechflu.2011.09.006, 2012.

Csanady, G. T.: Turbulent interface layers, Journal of Geophysical Research: Oceans, 83, 2329–2342, 1978.

Ellison, T. and Turner, J.: Turbulent entrainment in stratified flows, Journal of Fluid Mechanics, 6, 423–448, 1959.

Fer, I., Lemmin, U., and Thorpe, S.: Winter cascading of cold water in Lake Geneva, Journal of Geophysical Research: Oceans, 107, 2002.

Ferreira, R. M.: The von Kármán constant for flows over rough mobile beds. Lessons learned from dimensional analysis and similarity, Advances in Water Resources, 81, 19–32, 2015.

Ferreira, R. M., Franca, M. J., Leal, J. G., and Cardoso, A. H.: Flow over rough mobile beds: Friction factor and vertical distribution of the longitudinal mean velocity, Water Resources Research, 48, 2012.

Franca, M. and Lemmin, U.: Eliminating velocity aliasing in acoustic Doppler velocity profiler data, Measurement Science and Technology, 17, 313, 2006.

Goring, D. G. and Nikora, V. I.: Despiking acoustic Doppler velocimeter data, Journal of Hydraulic Engineering, 128, 117–126, 2002.

Huppert, H. E.: Gravity currents: a personal perspective, Journal of Fluid Mechanics, 554, 299–322, 2006.

Hurther, D. and Lemmin, U.: A correction method for turbulence measurements with a 3D acoustic Doppler velocity profiler, Journal of Atmospheric and Oceanic Technology, 18, 446–458, 2001.

Khavasi, E., Afshin, H., and Firoozabadi, B.: Effect of selected parameters on the depositional behaviour of turbidity currents, Journal of Hydraulic Research, 50, 60–69, 2012.

Kneller, B. and Buckee, C.: The structure and fluid mechanics of turbidity currents: a review of some recent studies and their geological implications, Sedimentology, 47, 62–94, 2000.

Lemmin, U. and Rolland, T.: Acoustic velocity profiler for laboratory and field studies, Journal of Hydraulic Engineering, 123, 1089–1098, 1997.

Lofquist, K.: Flow and stress near an interface between stratified liquids, The Physics of Fluids, 3, 158–175, 1960.

Maxworthy, T.: Experiments on gravity currents propagating down slopes. Part 2. The evolution of a fixed volume of fluid released from closed locks into a long, open channel, Journal of Fluid Mechanics, 647, 27–51, 2010.

Maxworthy, T. and Nokes, R.: Experiments on gravity currents propagating down slopes. Part 1. The release of a fixed volume of heavy fluid from an enclosed lock into an open channel, Journal of Fluid Mechanics, 584, 433–453, 2007.

Mulder, T. and Alexander, J.: Abrupt change in slope causes variation in the deposit thickness of concentrated particle-driven density currents, Marine Geology, 175, 221–235, 2001.

Nezu, I., Nakagawa, H., and Jirka, G. H.: Turbulence in open-channel flows, Journal of Hydraulic Engineering, 120, 1235–1237, 1994.

Niño, Y. and Garcia, M.: Experiments on particle—turbulence interactions in the near–wall region of an open channel flow: implications for sediment transport, Journal of Fluid Mechanics, 326, 285–319, 1996.

Nogueira, H. I., Adduce, C., Alves, E., and Franca, M. J.: Dynamics of the head of gravity currents, Environmental Fluid Mechanics, 14, 519–540, 2014.

Palmieri, A., Shah, F., and Dinar, A.: Economics of reservoir sedimentation and sustainable management of dams, Journal of Environmental Management, 61, 149–163, 2001.

Parker, G., Garcia, M., Fukushima, Y., and Yu, W.: Experiments on turbidity currents over an erodible bed, Journal of Hydraulic Research, 25, 123–147, 1987.

Salim, S., Pattiaratchi, C., Tinoco, R., Coco, G., Hetzel, Y., Wijeratne, S., and Jayaratne, R.: The influence of turbulent bursting on sediment resuspension under unidirectional currents, Earth Surface Dynamics, 5, 399, 2017.

Schleiss, A. J., Franca, M. J., Juez, C., and De Cesare, G.: Reservoir sedimentation, Journal of Hydraulic Research, 54, 595–614, 2016.

Simpson, J. E.: Effects of the lower boundary on the head of a gravity current, Journal of Fluid Mechanics, 53, 759–768, 1972.

Simpson, J. E.: Gravity currents: In the environment and the laboratory, Cambridge university press, 1997.

Stagnaro, M. and Pittaluga, M. B.: Velocity and concentration profiles of saline and turbidity currents flowing in a straight channel under quasi-uniform conditions, Earth Surface Dynamics, 2, 167, 2014.

Traer, M., Hilley, G., Fildani, A., and McHargue, T.: The sensitivity of turbidity currents to mass and momentum exchanges between these underflows and their surroundings, Journal of Geophysical Research: Earth Surface, 117, 2012.

Turner, J. S.: Buoyancy effects in fluids, Cambridge University Press, 1973.

Ungarish, M.: An introduction to gravity currents and intrusions, CRC Press, 2009.

Zordan, J., Schleiss, A. J., and Franca, M. J.: Bed shear stress estimation for gravity currents performed in laboratory., Proc. of River Flow 2016, St. Louis, USA, 855-861., 2016.

Zordan, J., Juez, C., Schleiss, A. J., and Franca, M. J.: Entrainment, transport and deposition of sediment by saline gravity currents, Advances in Water Resources, 2018a.

Zordan, J., Schleiss, A. J., and Franca, M. J.: Structure of a dense release produced by varying initial conditions, Environmental Fluid Mechanics, 2018b.